Developing FOB-CTMQC for use in simulating charge transport in organic semiconductors

Matt Ellis

Supervisor: Jochen Blumberger

Second Supervisor: Graham Worth

MPhil Upgrade Report

Department of Physics and Astronomy

University College London

January 8, 2019

Abstract

I am going to write the abstract last so as I imagine it will change as I edit the document.

Contents

Chapter 1

Introduction

1.1 Charge Transport Regimes in Organic Semiconductors

1.1.1 Organic Semiconductors

Conductive polymers were first discovered in 1977 by Shirakawa et al [1, 2] for which they were awarded the Nobel prize in Chemistry. Recently these materials have become ubiquitous in many technologies, such as in organic solar cells[3], organic field-effect transistors (OFET) [4] and organic light-emitting diodes (OLED) [5]. While the other two technologies lag behind their inorganic counterparts, uptake of OLED screens is becoming increasingly popular -especially in the smartphone and television market due to their flexibility, better colour reprsentation and lower energy consumption than standard backlit LCD displays. In fact IHS markit's OLED market tracker predicts OLED to be the dominant technology in smartphone screens by 2020 [6]. OLEDs have also found uses in lighting with their efficiency rivalling that of fluorescent tubes [7, 8]. Although, industry has made large strides in fabricating and using these materials the exact nature of the charge transport is still poorly understood. Conventional hopping and band theories break down in the regime of partial delocalisation of the charge carriers and atomistic simulations are required for a realistic picture.

Typically charge carrier mobilities in 'good' organic semiconductors (OSCs) fall between 1-10 $cm^2\ V^{-1}s^{-1}$ [9]. This is just beyond the range of hopping model validity ($\sim 1\ cm^2\ V^{-1}s^{-1}$) and below that of band theory ($> 50\ cm^2\ V^{-1}s^{-1}$) [10]. In this intermediate regime the charge carriers are typically not completely delocalised at the valence band edges (band regime) or localised to a single site/molecule (hopping regime) but delocalised over a few molecules. Without any analytic

approaches currently being valid in this regime many computational approaches have been developed to investigate the underlying charge transport mechanisms [11].

1.1.2 Band-like Transport

For high mobility, inorganic, semi-conducting materials such as Silicon and Germanium some variation on band theory can be applied. As large numbers of atoms come together to form a crystal their atomic orbitals overlap [12]. Due to the Pauli exclusion principle the energy level of the orbitals have to split to prevent any atoms having the same four quantum numbers. In a crystal with many atoms this splitting produces bands of energy separated by tiny values, effectively creating a continuum. In an inorganic semiconducting crystal the lattice sites (ions) are positively charged and create a periodic potential. Bloch's theorem can therefore be applied and the Schrödinger equation can be solved (with some approximations) to find the allowed energy bands. In general, these allowed bands form to produce a forbidden band in which there are no energy levels. This is called the band gap.

The two important bands for charge transport in semiconductors are the conduction and valence bands. These are the 2 bands either side of the Fermi level -the energy level, at thermodynamic equilibrium, which has a 50% chance of being populated. In order to conduct, a material must have empty states for electrons to move into. Those with no empty states are called insulators. In terms of band theory this means that the band-gap between the valence and conduction bands is very large; resulting in totally full states in the valence band and totally empty states in the conduction band [13]. For a conductor the Fermi level is somewhere in the valence band making it partially full. This results in plenty of free states for the electrons to move into without having to cross a band gap. Semiconductors on the other hand do have a band gap but it is small enough to be overcome by thermal fluctuations. This puts conductivity in these materials somewhere between an insulator and conductor.

Although successful in describing mobilities in inorganic semiconducting materials the assumptions of band theory make its use fairly limited in most inorganic crystals. The validity of band theory is linked to the delocalisation of charge carriers across the material [11]. In many organic semiconductors the charge carrier is only partially delocalised. For Bloch's theorem to hold the crystal must

be periodic and uniform throughout. However, many organic crystals show some disorder [9, 14, 15]. Further the periodic potential felt by the electrons is assumed to be static and doesn't interact with phonons and other electrons etc... This requirement is often not fulfilled in organic semiconductors as the molecules comprising the crystal are often only held together with weak Van Der Waals forces and a fairly free to move around.

1.1.3 Hopping-like Transport

Hopping theories assume the charge carrier is localised on one site and can hop from site to site in a series of discrete hops [11]. There are various underlying mechanisms for this. For example, the presence of the charge carrier at a site can alter the nuclear geometry. This distorted nuclear geometry can make it harder for the charge carrier to move onto the next site, creating a metastable state and trapping the charge carrier. The deformation in the nuclear geometry is called a small polaron.

Polaronic hopping theories have been used to great success with rates provided by Marcus theories and their derivatives [16, 17]. One of the key tools used in visualising this process (assuming harmonic response) are the Marcus Parabolas. These show how the free energy and reaction coordinates change after a charge transfer i.e. from initial to final diabatic states. The term 'diabatic state' isn't well defined and can refer to different things in different formulations. In this work a diabatic state can be imagined as the charge carrier localised on a single molecule. This is discussed later in more detail in section 2

Figure 1.1 above defines various important quantities for calculating the mobility in materials displaying hopping-like transport. The initial parabola describes the change in free energy with respect to the reaction coordinate for the initial state, for example when the charge is located on site 1. The final parabola describes the change in free energy when the charge is located on site 2 e.g. when the charge has relocated to site 2. The transition state (TS) is a point where the energies of the initial and final states are the same. This degenerate point is the only point at which the charge can move from the initial to final state as other points would result in a non-zero jump in energy between the 2 parabolas. The diabatic activation energy $\Delta G^{\ddagger}$ defines the energy required to get to this transition state from the minima of the initial parabola. The driving force ΔG^{0} is the difference in minima of the

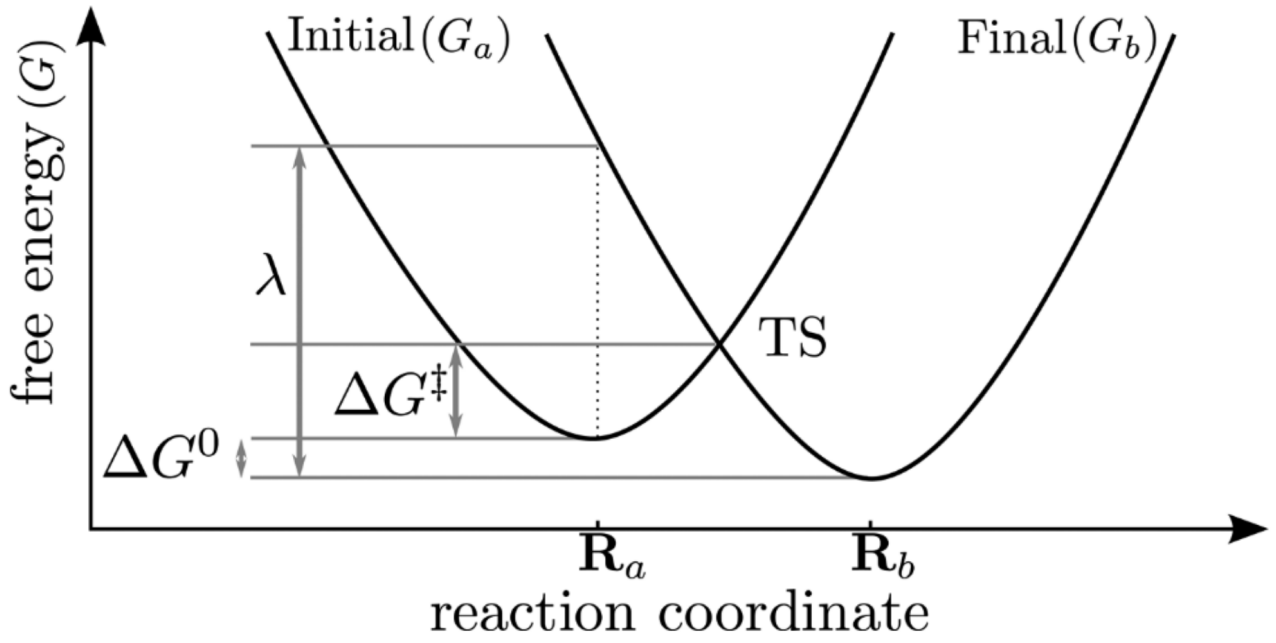

Figure 1.1: Marcus parabolas depicting the relationship between the free energy in the system and the reaction coordinate at 0 electronic coupling. This figure was taken from Oberhofer et al [11]

2 parabolas, the reorganisation energy λ defines the energy required to change the reaction coordinate from the final state minima to the initial state minima without changing electronic state.

Figure 1.1 can change when there is a non-zero electronic coupling (H_{ab}) between diabatic states. This parameter increases the chance of moving between the initial and final diabatic states by lowering the diabatic activation energy i.e. the energy required to transition from state 1 to 2. This is visualised in figure 1.2 In figure 1.2 above the diabatic activation energy has be lowered to $\Delta G^{\dagger} = \Delta G^{\ddagger} - H_{ab}$ making it easier for charge carriers to transition between diabatic states. In our formalism this means it is easier for charge carriers to move between sites i.e. delocalise. We see also that instead of being described totally by 2 parabolas there are 2 new adiabatic potential energy surfaces arising -the ground and excited state. The amount that these new potential energy surfaces diverge from the diabatic wells is dependent on an adiabaticity factor which is proportional to the ratio between the electronic coupling, H_{ab}, and the re-organisation energy, λ. This has been discussed in detail in multiple papers [11, 16, 18, 19] .

In fact for systems with couplings larger than $H_{ab} > \frac{3}{8}\lambda$ the diabatic activation energy vanishes

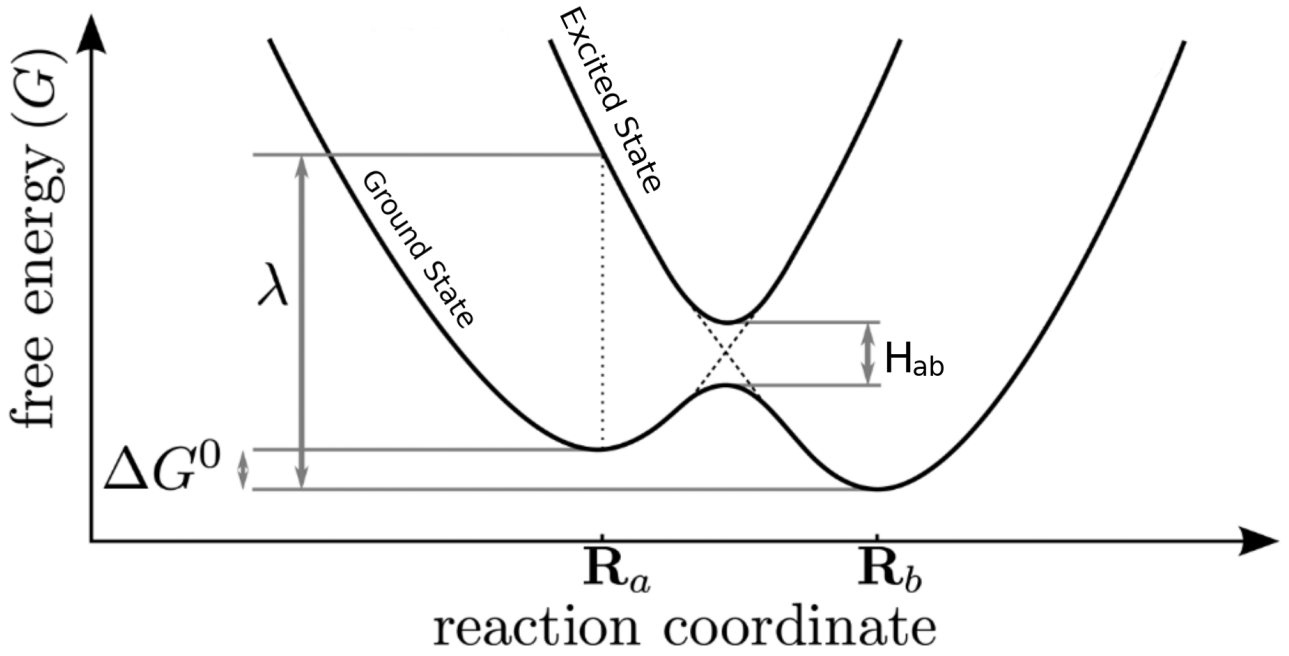

Figure 1.2: Graph depicting the change in free energy for a change in reaction coordinate for non-zero electronic coupling. Adapted from [11]

completely [16], meaning that there is no energy cost in transitioning between diabatic states. Beyond this regime hopping theories cannot be accurately applied. Unfortunately, at room temperatures thermal flucuations means the mean free path of the charge carriers is comparable to the intermolecular spacing. As such band theories too are inapplicable [11, 20, 21]. Much beyond this regime the energy cost to transition to higher adiabatic potential energy surfaces becomes prohibitively high and the system travels on a single state. In these situations the Born-Oppenhiemer approximation is valid. However, in this work I will be looking into the regime in between the band and hopping-like transport where we currently don't have analytical theories to describe charge transport. For this I will be using non-adiabatic atomistic simulations, namely coupled-trajectory mixed quantum classical molecular dynamics (CTMQC).

1.2 Atomisitc Simulations of Nonadiabatic Processes

In simulating processes involving electronic transfers a key approximation used in conventional molecular dynamics (MD) breaks down. That is the Born-Oppenheimer or adiabatic approximation [22]. This approximation, relied upon for almost a century [23], relies on the fact that nuclei are more massive than electrons and are approximately stationary with respect to electron movement [24]. This

results in nuclear evolution that is governed by a single, adiabatic, potential energy surface. However, in many interesting processes, such as electron transfer, non-radiative decay and photochemical processes, electronic transitions between adiabatic potential energy surfaces occur [25]. Simulating these processes requires non-adiabatic molecular dynamics (NAMD) techniques to be developed, to correctly capture dynamical properties.

There have been many techniques proposed for use in NAMD such as the quantum classical Louiville equation, multiple spawning [26] or nonadiabatic Bohmian dynamics [27]. However, two of the most popular are trajectory surface hopping [28] and mean-field approaches [29]. This is probably due to their relative simplicity to implement, efficiency for large systems and proven efficacy in a wide variety of situations. In all of these approaches the general aim is to treat as much of the system as possible with (computionally cheaper) classical mechanics. While handling all necessary parts with quantum mechanics [30]. In Surface Hopping, Ehrenfest and CTMQC one treats the nuclear subsystem classically and the electronic one quantum mechanically. The nuclei are propagated using a velocity verlet algorithm according to Newton's laws. The electrons are propagated using a fourth order Runge Kutta algorithm according to the time-dependent Schrödinger equation. This is normally expanded as a linear combination of adiabatic or diabatic states. The nuclei and electrons can also interact. Taking account of this interaction is where these different atomistic simulation techniques differ.

1.2.1 Surface Hopping and Ehrenfest Dynamics

In surface hopping, Ehrenfest and CTMQC dynamics the effect of the electrons on the nuclei is felt through the potential energy surface. In short the electronic populations control what the potential energy surface the nuclei are travelling on looks like. All the methods rely on a swarm of trajectories with slightly different initial conditions to sample configuration space.

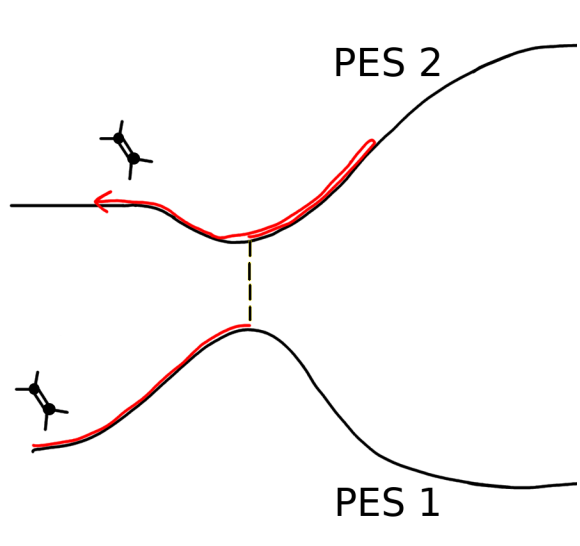

Figure 1.3: A cartoon of a surface hopping simulation near an avoided crossing. The black lines represent the adiabatic potential energy surface due to the ground and first excited state. The

In surface hopping the shape of the potential energy surface is determined by a series of discrete stochastic hops between adiabatic potential energy surfaces [31]. See fig 1.3.

The probability of these hops is determined by the non-adiabatic coupling between states. If this is high then a higher proportion of the total trajectories will hop if this is low then very few will. Although this method has been extremely successful, it has a few shortcomings. The original 'fewest switches surface hopping' proposed by John Tully suffered from bad overcoherence of the nuclear and electronic subsystems. That is the electronic and nuclear motion was coupled long after the region of high non-adiabatic coupling (crossing region). The fact that the hops are instant leads to discontinuities and methods need to be implemented to fix these such as velocity re-scaling. Finally, perhaps the most important shortcoming is that this technique has not been derived from first principles and cannot be guaranteed to work generally. These problems have lead to a number of other techniques being developed.

Another popular technique in the field of non-adiabatic dynamics is Ehrenfest dynamics (see fig). In this the nuclei travel on a potential energy surface that is a electronic population weighted average of the adiabatic potential energy surfaces. This technique, although derived from first principles, has a number of shortcomings of its own. The splitting of the nuclear wavefunction at crossing regions cannot be captured in Ehrenfest due to trajectories. Overcoherence is again a problem and it has been shown that at equilibrium all electronic states will be equally filled, violating detailed balance [32]. This also leads to an infinite electronic temperature in the limit of infinite electronic states.

1.2.2 Motivation for my Work

To overcome some of the challenges of the traditional Ehrenfest and Surface Hopping simulation techniques I plan to implement the newly proposed CTMQC technique [33]. This has been rigorously derived from the exact factorisation of the molecular wavefunction [34] and has been shown to work for toy model systems and a single molecule of Oxirane [33, 35]. The

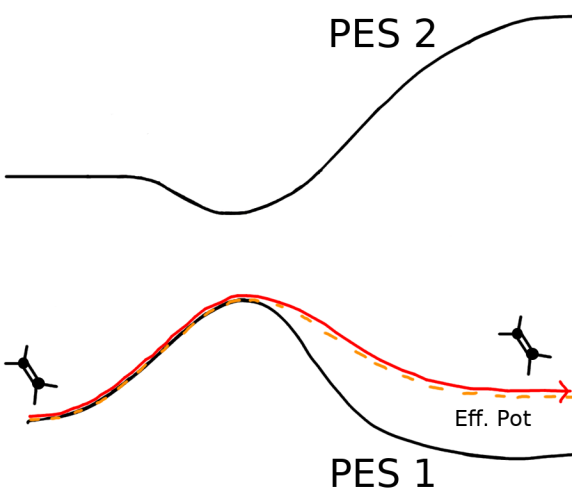

Figure 1.4: A cartoon of a Ehrenfest simulation near an avoided crossing. The black lines represent the adiabatic potential

equations appear to be the standard Ehrenfest equations with a correction provided by 2 new terms -the quantum momentum and a time-integrated adiabatic force. This correction allows a more theoretically rigorous handling of the decoherence and nuclear wavepacket splitting seen in nonadiabatic systems.

This technique should not be much more expensive than either surface hopping or Ehrenfest and when paired with a FOB formalism (see section 2) it should scale as $\mathcal{O}(N_{mol})$. Where N_{mol} is the number of molecules in the system. However, the approximations made in the derivation of CTMQC can be tuned to create a method fit for the system under consideration.

Chapter 2

FOB Formalism

The effect of the nuclei on the electrons is normally handled via the Hamiltonian. This is dependent on nuclear positions and is in turn used in the Schrödinger equation to propagate the electron dynamics. Often the construction of the Hamiltonian is carried out using density function theory (DFT). However, for large, dynamic systems this becomes too computationally expensive and a different technique should be used. In this work I will rely on an Analytical Overlap Method (AOM) [20] to calculate the off-diagonal elements of the Hamiltonian. The diagonal elements will be calculated via a forcefield.

2.1 AOM

AOM assumes that the off-diagonal elements of the Hamiltonian are proportional to the off-diagonal elements of the overlap matrix between 2 singly occupied molecular orbitals (SOMO) see figure 2.1. This is show in equation (2.1).

$$H_{kl} = CS_{kl} \tag{2.1}$$

This approximation was originally by Longuet-Higgins and Roberts [36] and its validity has been tested in our group previously in the small overlap regime [20]. Many of the presently most studied and promising organic semiconductors, such as Rubrene

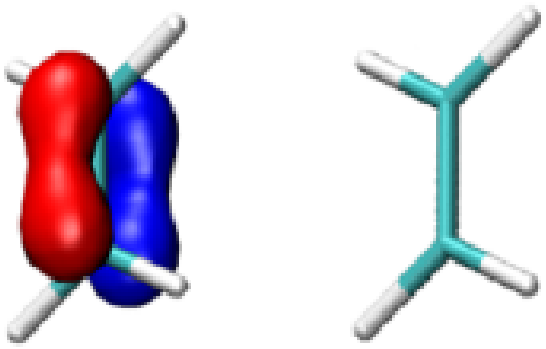

Figure 2.1: A depiction of a singly occupied molecular orbital (SOMO) on an ethylene molecule. Adapted from [18].

[37, 38] and Pentacene [39, 40] have pi-conjugation. In these systems it is often sufficient to include only 1 optimised p-orbital per atom [18]. This gives us an equation for the overlap of the SOMOs (φ_k) as:

$$S^{'}_{kl} = \langle \varphi_k | \varphi_l \rangle = \sum_{i \in k}^{atoms} \sum_{j \in l}^{atoms} c^{*}_{p\pi,i} c_{p\pi,j} \langle p_{\pi,i} | p_{\pi,j} \rangle \tag{2.2}$$

Where $\langle p_{\pi,i}|$ represents the optimised Slater p-orbital and the $c_{p\pi,i}$ terms are the AOM expansion coefficients. The gradient of the Hamiltonian can also be expressed in terms of the gradient of the overlap $\nabla_\nu H_{kl} = C \nabla_\nu S_{kl}$ (where ν represents the atom index). Further efficiencies can be made by expressing the gradient of the overlap in terms of (diabatic) NACVs e.g:

$$\nabla_\nu H^{'}_{kl} = C\, \nabla_\nu S^{'}_{kl} = C\, \nabla_\nu \langle \varphi_k | \varphi_l \rangle = C(\mathbf{d}^{'*}_{\nu,lk} + \mathbf{d}^{'}_{\nu,kl}) \tag{2.3}$$

Where we have defined the non-adiabatic coupling vectors (in a non-orthogonal diabtic basis) as $\mathbf{d}^{'}_{\nu,lk} = \langle \varphi_l | \nabla_\nu \varphi_k \rangle$. The $H^{'}_{kl}$ term is the Hamiltonian in the non-orthogonal diabatic basis. The NACVs are calculated via a fintie difference method.

2.2 Different Bases

The definitions in the previous section giving the key points in the AOM method were all expressed in a non-orthogonal diabatic basis. However, the electronic propagation in the FOB method is done in an orthogonal diabatic basis denoted ϕ_l. Further the CTMQC equations have been derived and are expressed in the adiabtic basis, ψ_l. Therefore, it is important to define the transformations between the 3 bases used in the code.

2.2.0.1 Basis Expansion

The time-dependent electronic wavefunction can be expressed as a linear combination of basis functions with expansion coefficients determining the size of their contribution. For example:

$$\Phi_{\mathbf{R}}(\mathbf{r},t) = \sum_{n}^{N_{states}} C_n(\mathbf{R},t) \psi_{\mathbf{R},n}(\mathbf{r}) = \sum_{l}^{N_{states}} u_l(\mathbf{R},t) \phi_{\mathbf{R},l}(\mathbf{r}) \tag{2.4}$$

Where $\Phi_{\mathbf{R}}(\mathbf{r},t)$ is the electronic wavefunction in the exact factorisation formalism. The subscript $\mathbf{R}$ denotes a parametric dependence on nuclear coordinates, the subscript n denote adiabatic state n similarly l denotes the l^{th} (orthogonal) diabatic state. Throughout this document I will use the

following naming convention: **R** denotes nuclear coordinates and **r** for the electronic coordinates. The C_l is the l^{th} adiabatic state. The squared modulus of this gives the population of electrons on that state. Expressing the electronic wavefunction in this way allows us to rewrite the propagation equations in terms of the expansion coefficients C_l or u_l.

As the propagation equations are written in terms of the expansion coefficients it is sensible to give the transformation equation in terms of them. To transform from the adiabatic to diabatic basis we can use the following unitary transformation:

$$\vec{C}(\mathbf{R},t) = \mathbb{U}(\mathbf{R},t)\ \vec{u}(\mathbf{R},t) \tag{2.5}$$

Here we have expressed the expansion coefficients as a vector e.g. $\vec{C} = \begin{pmatrix} C_1 \\ \vdots \\ C_n \end{pmatrix}$ The unitary transformation matrix is given as the overlap between diabatic and adiabatic states, $U_{ln} = \langle \phi_l | \psi_n \rangle$, and is a square matrix of size N^2_{states}. This is obtained by diagonalising the Hamiltonian in the code. The fact that this matrix is unitary means transforming from the diabatic to adiabatic is no more computationally expensive. The transformation can be obtained by pre-multiplying both sides of eq (2.5) by $\mathbb{U}^\dagger$ e.g.

$$\mathbb{U}^\dagger(\mathbf{R},t)\vec{C}(\mathbf{R},t) = \vec{u}(\mathbf{R},t) \tag{2.6}$$

To trasform from the non-orthogonal to orthogonal basis we need a new matrix. This is given by:

$$\vec{\phi} = \mathbb{T}\vec{\varphi} \tag{2.7}$$

This transformation is needed when transforming the non-orthogonal diabatic Hamiltonian, $H^{'}$, and non-adiabatic coupling terms to the orthogonal diabatic basis. For example, the orthogonal diabatic Hamiltonian is calculated as $H_{kl} = \left[\mathbb{T}^{-1}\mathbb{H}^{'}\mathbb{T}\right]_{kl}$. This matrix is equal to the inverse square of the overlap between SOMOs i.e. $T_{ml} = [\mathbb{S}^{-\frac{1}{2}}]_{ml}$.

Replacing the full charge transfer determinant with parametrised singly occupied molecular orbitals (SOMOs) makes the calculation of the relevant terms in the propagation of the system very efficient. The approximation has been scrutinised before in the group [16, 18–20, 41, 42] and its first implementation within the surface hopping framework has been shown to reproduce known phenomena such as the crossover from band-like to hopping-like transport [41]. In this way the interaction of the nuclei on the electrons is accounted for, as the overlap between SOMOs (and therefore the coupling, H_{ab}) depends on the nuclear geometry.

Chapter 3

CTMQC

3.1 Exact Factorisation

CTMQC comes from taking the semi-classical limit of an exact factorisation of the molecular wavefunction into its constituent electronic and nuclear components [34]. Where the electronic component is parametrically dependent on the nuclear coordinates, **R**. This is shown below in eq (3.1) where χ is the nuclear wavefunction and Φ is the electronic one.

$$\Psi(\mathbf{R},\mathbf{r},t) = \Phi_{\mathbf{R}}(\mathbf{r},t)\chi(\mathbf{R},t) \tag{3.1}$$

In the above equation (and throughout this report) I will denote nuclear coordinates and electronic coordinates *R* and *r* respectively. The nuclear and electronic wavefunctions then obey separate, but coupled, time-dependent schrödinger equations for spatial and temporal evolution. This representation has proven to be useful in furthering understanding through exact solutions of small toy-model systems (need ref [1]). However, in this report I will be focussing on the semi-classical limit of these equations (CTMQC) and give some early results of a combination of this and the AOM method explained previously in section 2. The equations for the evolution of the electronic and nuclear wavefunctions in the exact factorisation [34] are given below:

$$i\hbar\frac{\delta}{\delta t}\Phi_{\mathbf{R}}(\mathbf{r},t) = \left(\hat{H}_{BO} + \hat{U}_{en}[\Phi_{\mathbf{R}},\chi] - \varepsilon(\mathbf{R},t)\right)\Phi_{\mathbf{R}}(\mathbf{r},t) \tag{3.2}$$

$$i\hbar\frac{\delta}{\delta t}\chi(\mathbf{R},t) = \left(\sum_{\nu=1}^{N_n}\frac{[-i\hbar\nabla_\nu + \mathbf{A}_\nu(\mathbf{R},t)]^2}{2M_\nu} + \varepsilon(\mathbf{R},t)\right)\chi(\mathbf{R},t) \tag{3.3}$$

[1] see deconstruction paper

Where $\hat{H}_{BO}$ is the Born-Oppenheimer Hamiltonian, that is $\hat{T}_e + \hat{W}_{ee} + \hat{W}_{nn} + \hat{V}_{en}$. Where $\hat{T}_e$ is the electronic kinetic energy operator, $\hat{W}_{ee/nn}$ is the electron-electron/nuclei-nuclei interation and V_{en} is the electronic-nuclear potential.

The $\hat{U}_{en}$ is an electronic-nuclear coupling operator (ENCO). This is defined as

$$\hat{U}_{en}[\Phi_{\mathbf{R}},\chi] = \sum_{\nu=1}^{N_{nuc}} \frac{1}{M_\nu}\left[\frac{[-i\hbar\nabla_\nu - \mathbf{A}_\nu(\mathbf{R},t)]^2}{2} + \left(\frac{-i\hbar\nabla_\nu\chi}{\chi} + \mathbf{A}_\nu(\mathbf{R},\mathbf{t})\right)\left(-i\hbar\nabla_\nu - \mathbf{A}_\nu(\mathbf{R},t)\right)\right] \tag{3.4}$$

Where the $\mathbf{A}_\nu$ is a time-dependent vector potential (TDVP), given by $\langle\Phi_{\mathbf{R}}(t)|\, -i\hbar\nabla_\nu\Phi_{\mathbf{R}}\rangle_{\mathbf{r}}$ and M_ν is the mass of nuclei ν. Finally $\varepsilon(\mathbf{R},t)$ is a time-dependent scalar potential energy surface (TDPES), given by $\langle\Phi_{\mathbf{R}}(t)|\hat{H}_{BO} + \hat{U}_{en}^{coup} - i\hbar\frac{\delta}{\delta t}|\Phi_{\mathbf{R}}(t)\rangle_{\mathbf{r}}$.

The effects of the TDPES, TDVP and the ENCO have been investigated in multiple works [35, 43–46]. The TDPES and TDVP are both responsible for the evolution of the system [44]. The TDPES provides exact classical forces on the nuclei. In fact, an alternative independent-trajectory semi-classical scheme has been investigated using these exact forces [43]. This found the TDPES is responsible for the splitting of the nuclear wavepacket in regions of high non-adiabaticity by taking the shape of a step function between the 2 adiabatic potentials. This is demonstrated in figure 3.1. Finally the electronic-nuclear coupling operator (ENCO) is responsible for other non-adiabatic effects in the system such as electronic geometric diabtic transitions and decoherence [44].

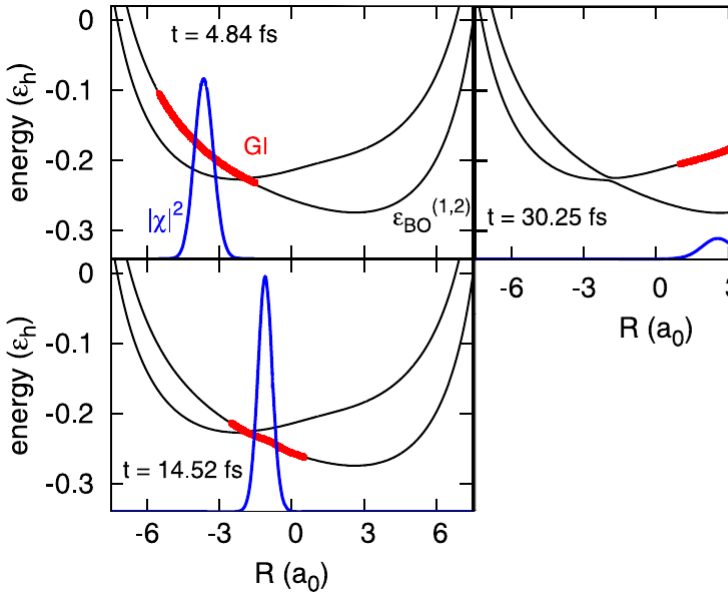

Figure 3.1: A demonstration of how the TDPES can cause the splitting of the nuclear wavepacket in non-adiabatic regions. The red line represents the TDPES and the blue is the nuclear density. Adapted from [43]

3.2 Approximations in CTMQC

Six approximations have been made in the derivation of CTMQC, these are discussed in detail in Ref. [33]. In the interest of completeness I have summarised them below.

3.2.1 Classical Nuclei

Techniques that include nuclear quantum effects (NQEs); such as multiple spawning [26], ring-polymer surface hopping [47] and nonadiabatic Bohmian dynamics [48, 49] although extremely accurate, cannot be applied to hundreds or thousands of molecules. This is due to their high computational cost. Further, in many systems of interest NQEs are negigible, especially at room temperature. For this reason the classical limit of the nuclear Schrödinger equation (3.3) is taken when deriving the CTMQC equations.

3.2.2 Neglect the ENCO in the TDPES

The electron-nuclei coupling operator is omitted in the expression for the time-dependent potential energy surface. This is justified as the first term ($[-i\hbar\nabla_\nu - \mathbf{A}_\nu(\mathbf{R},t)]^2$) contains a second order derivative which is expensive to calculate and has a neglible effect compared to the second term in the ENCO [50]. However, the rest of the ENCO is equal to zero when averaged over $\Phi_{\mathbf{R}}(\mathbf{r},t)$ so it does not contribute to the TDPES.

3.2.3 Derivative of the Adiabatic Coefficients

The derivative of the adiabatic coefficients appears in the electronic evolution equations. However, we can re-write the derivative of the adiabatic coefficients in terms of their modulus and phase:

$$\nabla_\nu C_l^{(I)}(t) = \left[\underbrace{\frac{\nabla_\nu |C_l^{(I)}(t)|}{|C_l^{(I)}(t)|}}_{\text{(Term 1)}} + \underbrace{\frac{i}{\hbar}\nabla_\nu \gamma_l^{(I)}(t)}_{\text{(Term 2)}} \right] C_l^{(I)}(t) \tag{3.5}$$

It has been found that the first term is negligible compared to the second [35, 43, 45] so it doesn't need to be calculated and we can remove it. It was also assumed that the NACVs are localised in space meaning that, after some algebra, the spatial derivative of the adiabatic coefficient can be written as:

$$\nabla_\nu C_l^{(I)}(t) = \frac{i}{\hbar}\nabla_\nu \gamma_l^{(I)}(t) C_l^{(I)}(t) = -\frac{i}{\hbar}\int^t dt' \nabla_\nu \varepsilon_l^{(I)} C_l^{(I)}(t) = -\frac{i}{\hbar}\mathbf{f}_l^{(I)} C_l^{(I)}(t) \tag{3.6}$$

Where $\varepsilon_l^{(I)}$ is the energy of the lth adiabatic potential energy surface for trajectory I, $C_l^{(I)}$ is the adiabatic expansion coefficient for state l and trajectory I. The $\mathbf{f}_l^{(I)}$ is the time-integrated adiabatic force.

3.2.4 Gaussian Nuclear Wavepackets

In order to calculate the quantum momentum -the new term in CTMQC. Knowledge of the nuclear distribution is needed. To this end the nuclear wavepacket is assumed to take the shape of a Gaussian. This is centred on the atomic coordinate with a width σ. In this work I have used a constant width throughout, with plans to implement dynamic Gaussian width calculations later. However, the nuclei are still propagated classically, the width parameter is only used in the calculation of the quantum momentum.

3.2.5 Seperating the Effects of Decoherence and NACVs

So as to not introduce any population transfer (due to the quantum momentum) when the NACV is zero a fifth approximation has been introduced. Namely the quantum momentum depends on pairs of states -l,k. This enables the seperation of the 'competing' effects of the NACV and the Quantum Momentum.

3.3 The CTMQC equations

3.3.1 Adiabatic Basis

The equations for the propagation of the classical nuclei and the expansion coefficients in the CTMQC framework in the adiabatic basis are given below:

$$\dot{\mathbf{P}}_\nu^{(I)} = \overbrace{-\sum_k |C_k^{(I)}|^2 \nabla_\nu \varepsilon_k^{(I)} - \sum_{k,l} C_l^{(I)} C_k^{*(I)} \left(\varepsilon_k^{(I)} - \varepsilon_l^{(I)}\right)}^{\text{Ehrenfest}} \underbrace{-\sum_{l,k} |C_l^{(I)}|^2 \left(\sum_{\nu'=1}^{N_n} \frac{2}{\hbar M_{\nu'}} \mathscr{Q}_{lk,\nu}^{(I)} \cdot \mathbf{f}_{l,\nu}^{(I)}\right) \left[|C_k^{(I)}|^2 \mathbf{f}_{k,\nu}^{(I)} - \mathbf{f}_{l,\nu}^{(I)}\right]}_{\text{Quantum Momentum}} \tag{3.7}$$

$$\dot{C}_l^{(I)} = \overbrace{-\frac{i}{\hbar}\varepsilon_l^{(I)} C_l - \sum_k C_k^{(I)} d_{lk}^{ad\ (I)}}^{\text{Ehrenfest}} \underbrace{- \sum_{\nu=1}^{N_n} \sum_k \frac{\mathscr{Q}_{lk,\nu}^{(I)}}{\hbar M_\nu} \cdot \left[\mathbf{f}_{k,\nu}^{(I)} - \mathbf{f}_{l,\nu}^{(I)}\right] |C_k^{(I)}|^2 C_l^{(I)}}_{\text{Quantum Momentum}} \tag{3.8}$$

Where the ε_k term is the potential energy on the kth potential energy surface. C_l is the adiabatic expansion coefficient corresponding to the lth state. The sum over k and l indicates a sum over all states, the (I) superscript is a replica index and the ν is an atom index. M_ν is the nuclear mass and $d_{lk}{}^{(}I)$ represents the non-adiabatic coupling element (in the adiabtic basis) between adiabatic states l and k, $\langle \psi_l | \frac{d}{dt} \psi_k \rangle$. The 2 new terms in this scheme not seen in other one are the $\mathscr{Q}_{lk,\nu}^{(I)}$ and the $\mathbf{f}_{k,\nu}^{(I)}$. These are the quantum momentum and the history dependent adiabatic force. The history dependent force in defined in equation (3.6) this keeps a record of the previous forces in the system. The quantum momentum term couples the trajectories together (making this a coupled-trajectory scheme). Together the history dependent force and quantum momentum are responsible for the decoherence in the 'Quantum Momentum' parts of the above equations [51]. Notably, although these equations have been derived from the exact factorisation equations separately from Ehrenfest they do contain exactly the Ehrenfest equations within them (marked 'Ehrenfest'). This scheme can therefore be seen as an Ehrenfest scheme with a correction that captures branching of the nuclear wavefunction and decoherence within it.

We can also see in equation (3.8) if we are in a pure adiabatic state i.e. all population on a single adiabatic state, there is no contribution from the quantum momentum part of the equations. In this scenario the evolution equations become simply Ehrenfest equations. For example, if we only have 1 state in the system with non-zero adiabatic population then the term $|C_k^{(I)}|^2 C_l$ is only non-zero when $l = k$. However, when $l = k$, the term $\left[\mathbf{f}_{k,\nu}^{(I)} - \mathbf{f}_{l,\nu}^{(I)}\right]$ is zero as $\mathbf{f}_{k,\nu}^{(I)} = \mathbf{f}_{l,\nu}^{(I)}$. Therefore, the quantum momentum term can be seen to only kick in when there is a mixing of adiabatic states. In the adiabatic formulation of these equations it is the adiabatic NACV $\mathbf{d}_{lk,\nu}^{ad,(I)}$ that is responsible for the initial mixing of the populations from pure adiabatic states.

3.3.2 Diabatic Basis

The equations above (3.7) & (3.8) are both in the adiabatic basis. However, to make use of the FOB-formalism detailed in section 2 already implemented in the CP2K software package [52] these need to be transformed to the orthogonal diabatic basis, ϕ. After applying the transformation matrix $\mathbb{U}$ and some algebra the equations in the diabatic basis can be written as:

$$F_v^{(I)}(t) = \overbrace{-\sum_{l,k} u_l^{(I)*} u_k^{(I)} \nabla_v H_{lk}^{(I)} - \sum_{l,k,a} d_{la}^{(I)} H_{ak}^{(I)} - d_{ak}^{(I)} H_{la}^{(I)}}^{\text{Ehrenfest}} \underbrace{-2\sum_l |C_l^{(I)}|^2 \sum_n \left(\sum_{v'}^{N} \frac{\mathscr{Q}_{ln,v'}^{(I)}(t)}{\hbar M_{v'}} \cdot \mathbf{f}_{l,v'}^{(I)} \right) \left[|C_n^{(I)}|^2 \mathbf{f}_{n,v}^{(I)} - \mathbf{f}_{l,v}^{(I)} \right]}_{\text{Quantum Momentum}} \tag{3.9}$$

$$\dot{u}_k^{(I)} = \overbrace{-\frac{i}{\hbar} \sum_l u_l^{(I)} \left(H_{kl}^{(I)} + \hbar d_{kl}^{(I)} \right)}^{\text{Ehrenfest}} \tag{3.10}$$

$$\underbrace{+\sum_s U_{ks} \sum_{v=1}^{N_n} \sum_n \frac{\mathscr{Q}_{sn,v}^{(I)}}{\hbar M_v} \cdot \left[\mathbf{f}_{n,v}^{(I)} - \mathbf{f}_{s,v}^{(I)} \right] |C_n^{(I)}|^2 \sum_l U_{sl}^* u_l^{(I)}}_{\text{Quantum Momentum}} \tag{3.11}$$

Where $u_l^{(I)}$ represents the diabatic expansion coefficient for (orthogonal) diabatic state l on trajectory I. $H_{kl}^{(I)} = \langle \phi_k^{(I)} | H^{(I)} | \phi_l^{(I)} \rangle$ is the diabatic Hamiltonian. $d_{kl} = \langle \phi_k^{(I)} | \dot{\phi_l^{(I)}} \rangle$ is the diabatic non-adiabatic coupling element (NACE). $U_{ks} = \langle \phi_k | \psi_s \rangle$ is the adiabatic-diabatic transformation matrix. The other terms have been previously defined (see section).

The 2 expressions can again be decomposed into a quantum momentum part and an Ehrenfest part. In the force expression (3.9) the Ehrenfest part comprises 2 terms. In tests I have found the first term contributes significantly more to the overall force than the second 'commutator' term. This means that the second term, can be neglected in most situations. The quantum momentum term in the force expression is expressed in the adiabatic basis. This is because it is basis independent and numerically transforming it with transformation matrices would result in unnecessary computation. The quantum momentum part of the electronic equation (3.11) is largely unchanged compared to the adiabatic one (3.8) and an on-the-fly transformation from adiabatic to diabatic representations is

required during propagation.

The diabatic hamiltonian, as opposed to the adiabatic one, now contains non-zero off-diagonal elements. This is the primary term responsible for population transfer when in pure adiabatic states. The diabatic NACE has a much smaller effect.

3.4 Calculating the Quantum Momentum

The technique for calculating the quantum momentum term is outlined in detail in the SI of [53]. The original equations given in [33] present a quantum momentum term without state indices (l,k). This, due to approximations made in the derivation of CTMQC, results in population transfer even when the non-adiabatic couplings between states are zero. Therefore Agostini et al has enforced this with the pair-wise state dependence of the quantum momentum.

The quantum momentum is defined as:

$$\mathscr{Q}_{\nu}(I) = \frac{-\hbar\nabla_{\nu}|\chi^{(I)}|}{|\chi^{(I)}|}\frac{-\hbar\nabla_{\nu}|\chi^{(I)}|^2}{2|\chi^{(I)}|^2} \tag{3.12}$$

In order to reconstruct the nuclear density Gaussian distributions can be used. This results in a linear expression for the quantum momentum. The full details of the derivation are given in the supplementary information of [53]. The resulting linear expression for the quantum momentum is given below:

$$\mathscr{Q}^{(I)}_{lk,\nu} = \alpha^{(I)}_{\nu}\mathbf{R}^{(I)}_{\nu} - \mathbf{R}_{lk,\nu} \tag{3.13}$$

Where $\mathbf{R}^{(I)}_{\nu}$ are the nuclear coordinates on trajectory I on atom ν. The $\alpha_{\nu}(I)$ term is a weighted average over trajectories of the product of the gaussian's assigned to each atomic coordinate, i.e:

$$\alpha^{(I)}_{\nu} = \sum_{J}^{N_{tr}} \frac{\hbar\prod_{\nu'} g_{\sigma^{(J)}_{\nu'}(t)}\left(\mathbf{R}^{(I)}_{\nu'}(t) - \mathbf{R}^{(J)}_{\nu'}(t)\right)}{2\sigma^{(J)}_{\nu}(t)^2\sum_{K}^{N_{tr}}\prod_{\nu'} g_{\sigma^{(K)}_{\nu'}(t)}\left(\mathbf{R}^{(I)}_{\nu'}(t) - \mathbf{R}^{K)}_{\nu'}(t)\right)} \tag{3.14}$$

Where $\sigma^{(J)}_{\nu'}(t)$ is a width parameter for the width of the gaussian centered at atomic coordinates. Along with the $\mathbf{R}_{lk,\nu}$ term the $\alpha^{(I)}_{\nu}$ performs the job of coupling the trajectories together. The $\mathbf{R}_{lk,\nu}$

term also given in the SI of [53] is defined for each cartesian dimension as:

$$R_{lk,\nu} = \sum_{I}^{N_{tr}} R_{\nu}^{(I)}(t)\alpha_{\nu}^{(I)}(t)\frac{|C_k^{(I)}(t)|^2|C_l^{(I)}(t)|^2\left(f_{k,\nu}^{(I)}(t) - f_{l,\nu}^{(I)}(t)\right)}{\sum_J |C_k^{(J)}(t)|^2|C_l^{(J)}(t)|^2\left(f_{k,\nu}^{(J)}(t) - f_{l,\nu}^{(J)}(t)\right)} \tag{3.15}$$

Where the bold notation for vectors has been replaced by normal font indicating that this applies to each cartesian dimension independently. Further, in this expression $R_{lk,\nu}$ is anti-symmetric, $R_{lk} = R_{kl}$ meaning that $Q_{lk} = Q_{kl}$. At first sight the R_{lk} term seems to be another weighted average. However, this isn't quite the case as the denominator can have negative terms. This causes equation (3.15) to be very sensitive to errors in the calculation of the denominator of this fraction. Any inaccuracies can lead to the denominator approaching zero faster than the numerator causing large spikes in the quantum momentum term.

3.5 Testing my Implementation

I have implemented a serial version of this algorithm in the CP2K software package [52]. As well as many numerical tests on individual terms in the equations, I have implemented some physical tests too. In this section I will outline some of the key physical tests I have performed on both the Ehrenfest part of the equations and the full CTMQC equations.

3.5.1 Rabi Oscillation

Rabi Oscillation can be shown to occur in systems that have fixed nuclear geometries (see section A.2). This can be used to check the electronic propagation, which is carried out using a fourth order Runge-Kutta algorithm. In this test I propagated the system with the Ehrenfest method and set velocities to zero, thus freezing the positions of the nuclei. I compared this to this to the analytically calculated coefficients using python and the Rabi Oscillation formula. The results are shown below in figure 3.2.

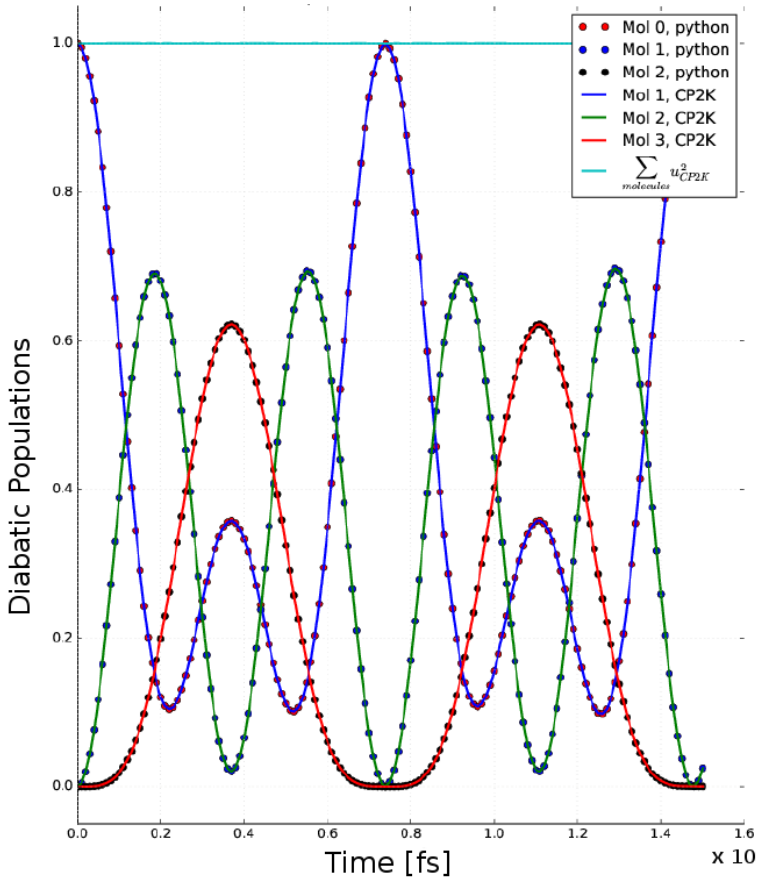

Figure 3.2: Rabi Oscillations occuring in a trimer of Ethylene-like molecules. Dots indicate the coefficient calculated by python according to the Rabi formula. Lines indicate the CP2K output. The different colours represent different diabatic states.

We can see in figure 3.2 CP2K gives the same output as the analytic result, meaning the Runge-Kutta method is working. The cyan line shows us the norm is preserved in this system.

3.5.2 Energy Conservation

Ehrenfest can be shown to conserve the potential energy + total kinetic energy [54]. The potential energy is given by the effective potential (i.e. $\sum_l |C_l^{(I)}|^2 \varepsilon_l$) and the total kinetic energy is given as a sum of the kinetic energy over all atoms. In this test the commutator term was neglected from equation (3.9). 8 simulations were performed. These used the same initial conditions but varied a random number generator seed, which is used in the calculation of the NACVs. In each simulation 100 replicas were used over various couplings and averaged to get the average energy drift per replica. The error bar was obtained from the average energy drifts of the 8 simulations.

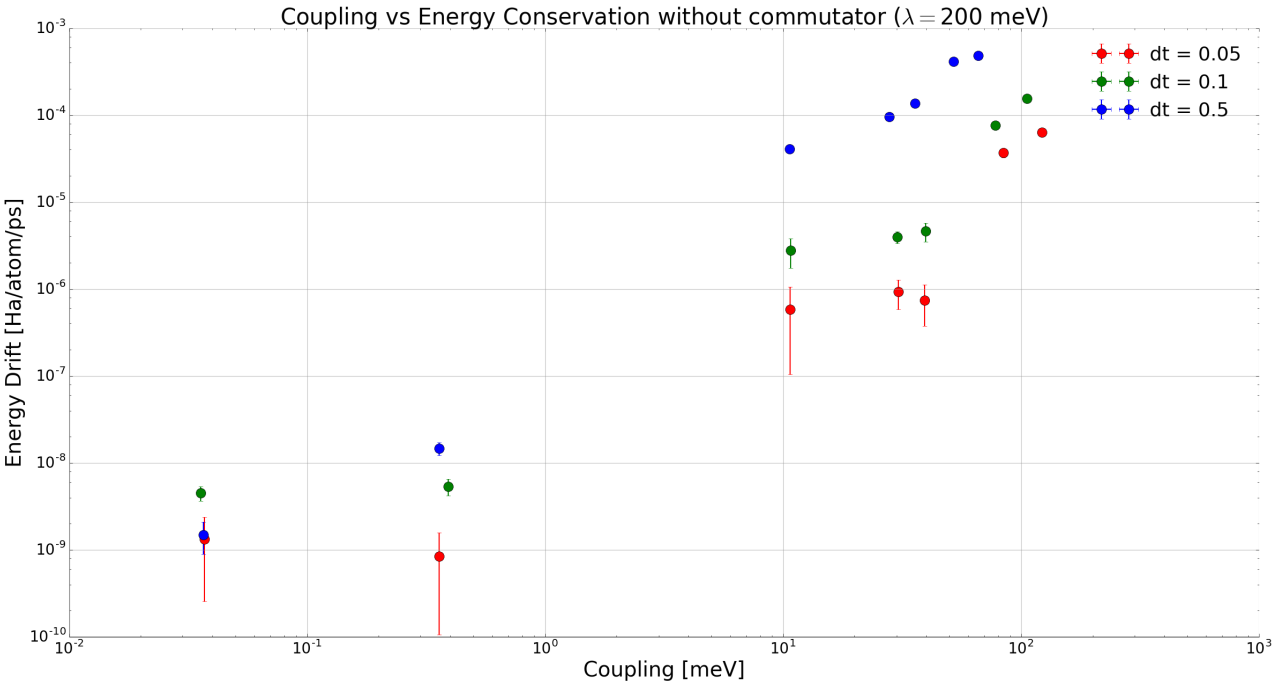

Figure 3.3: Energy drift in Ehrenfest for various couplings. Each color represents a different nuclear time-step used in fs.

We can see that the energy is conserved very well for low couplings and starts to increase for higher ones. The exact reason for this is not known. It may be due to the fact the the effective potential energy surface is a population weighted average. If the energies are closer together around the crossing region (as in lower coupling systems) then this average becomes a better representation of the true potential. When the states are further apart the average becomes more of an approximation. From this graph a time-step of 0.1fs was chosen as a compromise between accuracy and computational cost.

3.5.3 Norm Conservation

The norm of the coefficients should be conserved when propagating the equations. To not do so would mean that the total number of charge carrier is changing, i.e. electrons/holes being destroyed or created. Both the CTMQC and Ehrenfest electronic equations can be shown to conserve the norm (see appendix A.1). This is very well conserved in Ehrenfest, with norm drifts (using a nuclear time-step of 0.1fs) of the order 10^{-10} ps^{-1}. However, in CTMQC the story is slightly different.

The quantum momentum appears in both the nuclear force equation and the electronic equation.

However, its current formulation using Gaussian distributions to model the nuclear density results in equation (3.13). That is $Q^{(I)}_{lk,\nu} = \alpha^{(I)}_{\nu}\mathbf{R}^{(I)}_{\nu} - \mathbf{R}^{(I)}_{lk,\nu}$. Where the $\mathbf{R}^{(I)}_{lk,\nu}$ term is calculated via equation (3.15). This is given again below in a condensed form:

$$\mathbf{R}_{lk,\nu} = \sum_{I}^{N_{tr}} R^{(I)}_{\nu}(t)\alpha^{(I)}_{\nu}(t)\frac{\mathbf{Y}^{(I)}_{lk,\nu}(t)}{\sum_J \mathbf{Y}^{(I)}_{lk,\nu}(t)}$$

Where $\mathbf{Y}^{(I)}_{lk,\nu} = |C^{(J)}_k(t)|^2|C^{(J)}_l(t)|^2\left(\mathbf{f}^{(J)}_{k,\nu}(t) - \mathbf{f}^{(J)}_{l,\nu}(t)\right)$.

However, the $\mathbf{Y}^{(I)}_{lk,\nu}$ can be both negative and positive so after summing $\mathbf{Y}^{(I)}_{lk,\nu}$ over all replicas the denominator can approach zero. Any small inaccuracies in the propagation will result in large spikes in this term, thus causing bad norm conservation and unphysical data. A demonstration of this can be seen below.

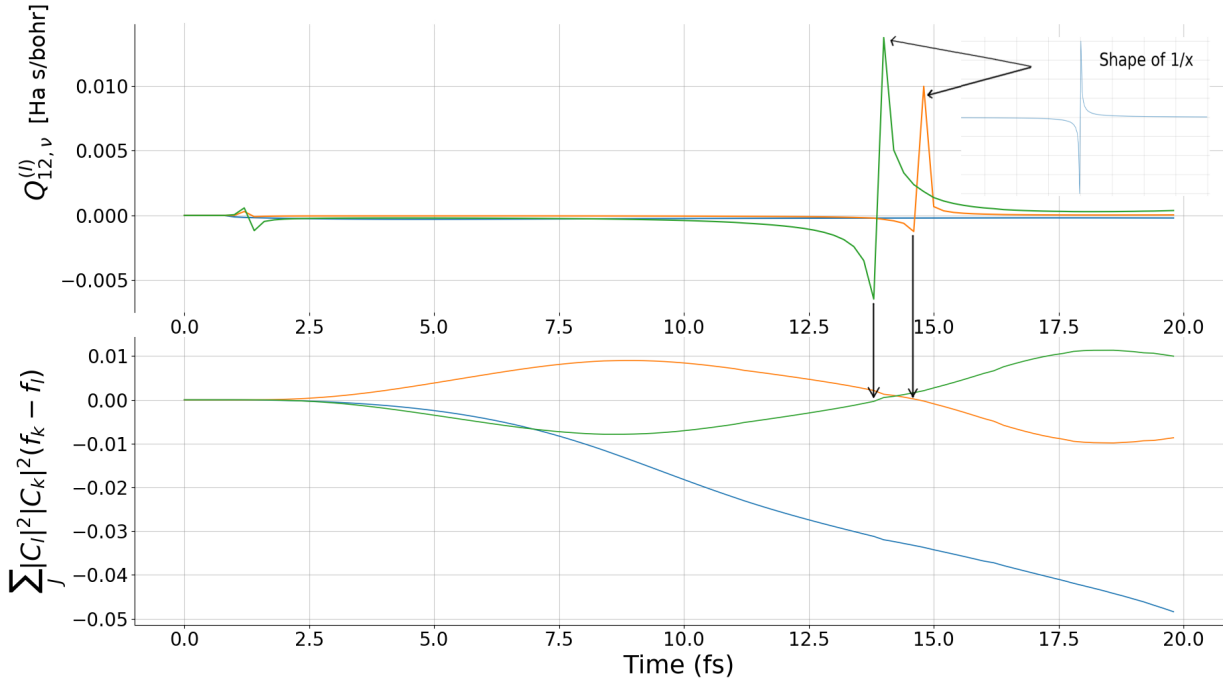

Figure 3.4: A time-series plot of the denominator in the $\mathbf{R}_{lk,\nu}$ equation (bottom graph) and the quantum momentum term between states 1 & 2 on atom 1 for replica 1 (top graph). Each colour represents a different cartesian component.

In figure 3.4 when the bottom part of the fraction approaches zero there is a spike in the quantum momentum. This spike in the quantum momentum then affects the nuclear and electronic propagation.

One way this manifests itself is in bad norm conservation. This is shown in figure below (3.5)

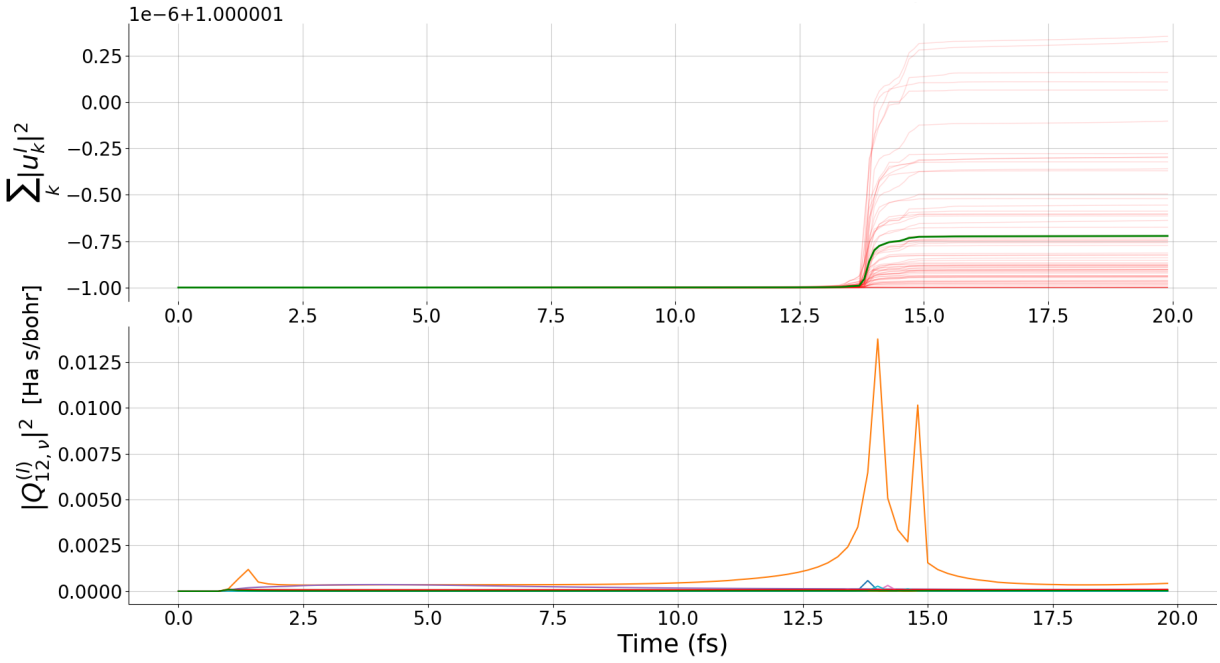

Figure 3.5: A time-series plot of the modulus of the quantum momentum between states 1 & 2 on atom 1 for replica 1 (bottom graph) and the norm of the diabatic expansion coefficients (top graph).

In an attempt to counter this problem a smoothing function has been implemented in the calculation of the $R_{lk,\nu}$ term. This takes the shape of a $\tanh()^2$ function, that is:

$$\mathbf{R}_{lk,\nu} = \sum_{I}^{N_{tr}} R_{\nu}^{(I)}(t)\alpha_{\nu}^{(I)}(t)\tanh\left(\frac{\sum_J \mathbf{Y}_{lk,\nu}^{(I)}(t)}{W}\right)^2 \frac{\mathbf{Y}_{lk,\nu}^{(I)}(t)}{\sum_J \mathbf{Y}_{lk,\nu}^{(I)}(t)} \tag{3.16}$$

By altering the 'width' parameter, W, one can set the level of smoothing of the spikes in the quantum momentum term. Lower widths result in less smoothing. After investigating various widths for various couplings a default width of 0.001 au_f has been chosen. This seems to provide a good balance between a norm conservation and physical dynamics. A width that is too high would result in a very low/neglible $\mathbf{R}_{lk,\nu}$ term. A very low width would result in very little smoothing and bad norm conservation. This parameter is something that should be monitored when working with different systems. Using the tanh smoothing improves the conservation of the norm by orders of magnitude and prevents the code from crashing.

3.5.4 Time-Derivative of the Sum Over Trajectories of Adiabatic Populations

In the supplementary information of Min, 17 [53] a further condition was imposed when deriving the equation for the Quantum Momentum (equation S26). This is given below:

$$\sum_{I}^{N_{rep}} \frac{d|C_{qm,l}^{(I)}|^2}{dt} = \sum_{I}^{N_{rep}} \sum_{\nu}^{N_n} 2 \frac{\mathscr{Q}_{lk,\nu}^{(I)}}{\hbar M_\nu} \cdot \left(\mathbf{f}_{k,\nu}^{(I)} - \mathbf{f}_{l,\nu}^{(I)}\right) |C_l^{(I)}|^2 |C_k^{(I)}|^2 = 0 \qquad \forall l,k \tag{3.17}$$

This equation can be used to monitor the dynamics and test the Quantum Momentum calculation. Figure 3.6 below shows the result of this for an arbitrary coupling (10meV) in a dimer of an Ethylene like molecule.

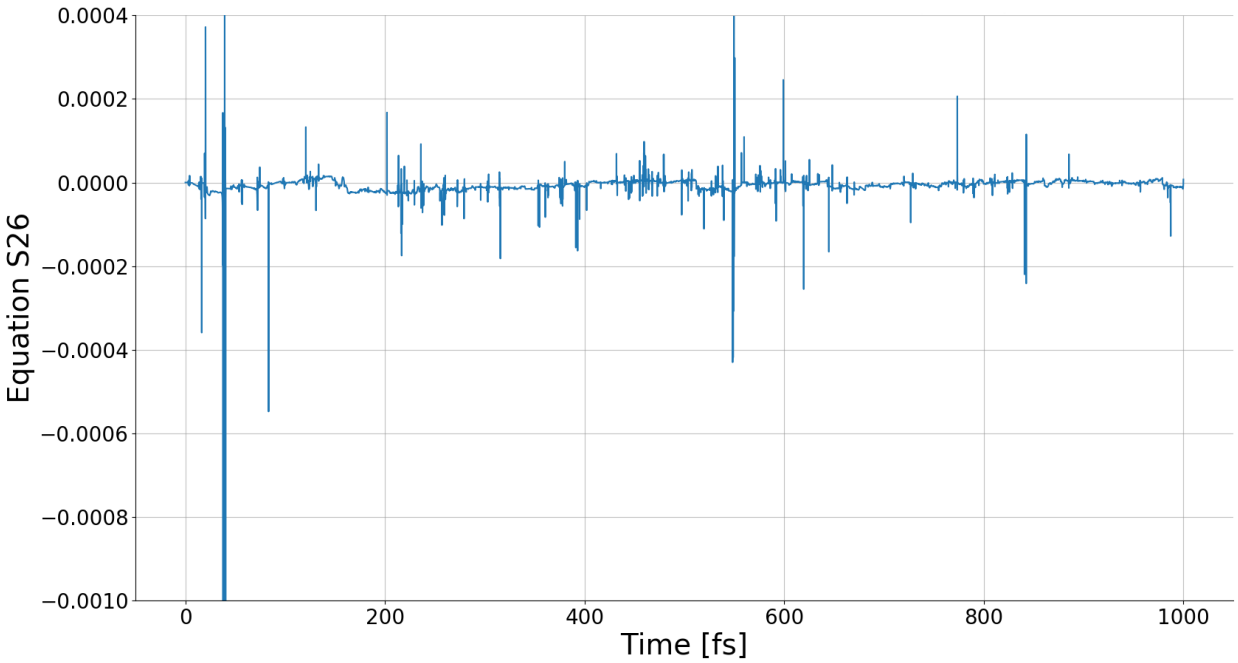

Figure 3.6: Equation S26 from [53]. A coupling of 10meV was used and a tanh smoothing width was 0.0001 au_f.

We can see that the equation is fulfilled to within $\sim 10^{-5}$ with some fairly large spikes. These spikes are caused by a spike in the quantum momentum due to denominator in the $\mathbf{R}_{lk,\nu}$ equation (3.15) approaching zero. This assures me that the quantum momentum is implemented correctly.

Chapter 4

General Conclusions

There are many real world applications of organic semiconductors and accurate models of charge transport are important to facilitate new materials discovery and characterisation. However, due to mobilities falling within an intermediate region where neither band theories nor hopping theories are applicable non-adiabatic atomistic simulations must be used. Among the litany of techniques proposed there are no single silver bullets. As always, the user must make the compromise between accurate dynamics and computational cost. Two of the most popular mixed-quantum classical techniques are trajectory surface hopping (TSH) and Ehrenfest. However, these both suffer from well known problems such as over-coherent nuclear-electronic dynamics no branching of the nuclear wavefunction in Ehrenfest and lack of a first-principles grounding in TSH.

To overcome these challenges a new technique, coupled-trajectory mixed-quantum classical molecular dynamics (CTMQC), has been proposed [44] to more rigorously account for decoherence, branching of the nuclear wavefunction and to provide a technique based in first principles physics. This technique, derived from the exact factorisation of the molecular wavefunction [34], appears as a 'corrected' Ehrenfest scheme where the correction comes from 2 new terms -an adiabatic time-integrated force and a quantum momentum.

In this report I have outlined an implementation of CTMQC paired with a fragment-orbital based (FOB) technique to produce an efficient FOB-CTMQC propagator capable of simulating hundreds of organic molecules. The FOB method is based on the assumption that the electronic couplings (off-diagonal Hamiltonian elements) are proportional to the overlap between singly occupied molec-

ular orbitals (SOMOs). This approximation has been validated in many organic semiconductors and provides a significant speed-up when compared to using density functional theory.

The implementation process is still under progress. However, initial results are promising. Some key tests have been discussed including Rabi oscillation, energy conservation, norm conservation and the fulfilment of a fundamental equation (3.17). The tests have been mostly positive. However, due a denominator in the equation for calculating the quantum momentum approaching zero -causing the quantum momentum to spike. The norm was not well conserved and a smoothing $\tanh^2$ function was used to fix this.

To build on this work I would now like to apply FOB-CTMQC to more realistic systems and to eventually compare with experimental results. In the short term, I will check whether detailed balance is upheld and compare this to an in house decoherence-corrected surface hopping scheme. I will be able to calculate rate constants for charge carrier mobilities in small chains. However, the fact that the implementation is a serial one imposes a severe restriction on the size of system I am able to study. Parallelising the code will enable me to progress past 10 molecules into the hundreds.

Appendix A

Derivations

A.1 Preservation of the Norm

A.1.1 Ehrenfest

The statement of the conservation of norm is:

$$\sum_{l}^{N_{states}} \frac{d}{dt}|C_l^{(I)}|^2 = 0$$

Using chain rule (and assuming this hold for each replica) we can write this as:

$$\sum_{l}^{N_{states}} \frac{d}{dt}|C_l|^2 = \left(\frac{d}{dt}C_l^*\right)C_l + C_l^*\left(\frac{d}{dt}C_l\right)$$

If we write, $C_l = (a+bi)$ and $C_l^* = (a-bi)$ we can see the following relation holds:

$$\sum_{l}^{N_{states}} \frac{d}{dt}|C_l|^2 = \sum_{l}^{N_{states}} \left(\frac{d}{dt}C_l^*\right)C_l + C_l^*\left(\frac{d}{dt}C_l\right) = \sum_{l}^{N_{states}} 2\mathscr{R}\left[C_l^*\left(\frac{d}{dt}C_l\right)\right]$$

We have an expression for the time-derivative of the adiabatic expansion coefficient, under Ehrenfest (equation (**??**)). Inserting this above we get:

$$\sum_{l}^{N_{states}} \frac{d}{dt}|C_l|^2 = \sum_{l}^{N_{states}} 2\mathscr{R}\left[C_l^*\frac{-i}{\hbar}C_l\varepsilon_l - \sum_k C_l^*C_k d_{lk}^{ad}\right]$$

The first term is imaginary so we can remove it, as we're only interested in the real components:

$$\sum_{l}^{N_{states}} \frac{d}{dt}|C_l|^2 = -2 \sum_{l,k}^{N_{states}} \mathscr{R}\left[C_l^* C_k d_{lk}^{ad}\right]$$

The next term is exactly zero due to the anti-symmetry of the NACE that is the equation above can be written as:

$$\sum_{l}^{N_{states}} \frac{d}{dt}|C_l|^2 = -2 \sum_{k=2}^{N_{states}} \sum_{l<k} \mathscr{R}\left[(C_l^* C_k - C_k^* C_l) d_{lk}\right] = 0$$

A.1.2 CTMQC

The proof of conservation of the norm in CTMQC is similar to Ehrnfest. Again we write:

$$\sum_{l}^{N_{states}} \frac{d}{dt}|C_l|^2 = \sum_{l}^{N_{states}} 2\mathscr{R}\left[C_l^* \left(\frac{d}{dt} C_l\right)\right]$$

This time, the propagtion equation is slightly different:

$$\sum_{l}^{N_{states}} \frac{d}{dt}|C_l|^2 = \sum_{l}^{N_{states}} 2\mathscr{R}\left[C_l^* \frac{-i}{\hbar} C_l \varepsilon_l - \sum_k C_l^* C_k d_{lk}^{ad} - \sum_{\nu=1}^{N_n} \sum_k \frac{\mathscr{Q}_{lk,\nu}^{(I)}}{\hbar M_\nu} \cdot \left(\mathbf{f}_{k,\nu}^{(I)} - \mathbf{f}_{l,\nu}^{(I)}\right) |C_k|^2 C_l^{(I)} C_l^{*\,(I)}\right]$$

We have seen that the Ehrenfest part of the above equation conserves the norm, so we can remove that. we can also combine the 2 C_l terms on the end:

$$\sum_{l}^{N_{states}} \frac{d}{dt}|C_l|^2 = -2 \sum_{l,k}^{N_{states}} \mathscr{R}\left[\sum_{\nu=1}^{N_n} \frac{\mathscr{Q}_{lk,\nu}^{(I)}}{\hbar M_\nu} \cdot \left(\mathbf{f}_{k,\nu}^{(I)} - \mathbf{f}_{l,\nu}^{(I)}\right) |C_k|^2 |C_l^{(I)}|^2\right]$$

Because $\mathscr{Q}_{lk,\nu}^{(I)} = \mathscr{Q}_{kl,\nu}^{(I)}$ (and the diagonal is undefined) we can re-write the above equation as:

$$\sum_{l}^{N_{states}} \frac{d}{dt}|C_l|^2 = -2 \sum_{l}^{N_{states}} \sum_{k<l} \mathscr{R}\left[\sum_{\nu=1}^{N_n} \frac{\mathscr{Q}_{lk,\nu}^{(I)}}{\hbar M_\nu} \cdot \left[\left(\mathbf{f}_{k,\nu}^{(I)} - \mathbf{f}_{l,\nu}^{(I)}\right) + \left(\mathbf{f}_{l,\nu}^{(I)} - \mathbf{f}_{k,\nu}^{(I)}\right)\right] |C_k|^2 |C_l^{(I)}|^2\right] = 0$$

So the norm should be conserved for each replica in CTMQC.

A.2 Rabi Oscillation

By only allowing one parameter to vary in the propagation one can isolate and test that. For the electronic propagation I held the nuclear positions constant resulting in rabi oscillation. This is due to the Schrödinger equation changing from a partial differential equation to, an analytically solvable, ordinary differential equation i.e:

$$i\hbar\frac{\delta}{\delta t}\Phi(\mathbf{R}(t),t) = \hat{H}(\mathbf{R}(t),t)\Phi(\mathbf{R}(t),t)$$

$$\downarrow$$

$$i\hbar\frac{d}{dt}\Phi(t) = \hat{H}(t)\Phi(t)$$

Which has the general solution:

$$\Phi(t) = e^{i\hbar\hat{H}t}\Phi(0)$$

Appendix B

Colophon

This document was set in the Time Roman typeface using LaTeXand BibTeX, composed with the Atom text editor. The Python programming language was used for all plots and data analysis.

Bibliography

[1] C. K. Chiang, C. R. Fincher, Y. W. Park, A. J. Heeger, H. Shirakawa, E. J. Louis, S. C. Gau, and Alan G. MacDiarmid. Electrical Conductivity in Doped Polyacetylene. *Physical Review Letters*, 39(17):1098–1101, October 1977.

[2] Hideki Shirakawa, Edwin J. Louis, Alan G. MacDiarmid, Chwan K. Chiang, and Alan J. Heeger. Synthesis of electrically conducting organic polymers: halogen derivatives of polyacetylene, (CH)x. *J. Chem. Soc., Chem. Commun.*, 0(16):578–580, Jan 1977.

[3] Bernard Kippelen and Jean-Luc Brédas. Organic photovoltaics. *Energy Environ. Sci.*, 2(3):251–261, 2009.

[4] M. J. Małachowski and J. Żmija. Organic field-effect transistors. *Opto-Electron. Rev.*, 18(2):121–136, Jun 2010.

[5] N. Thejo Kalyani and S. J. Dhoble. Organic light emitting diodes: Energy saving lighting technology—A review. *Renewable Sustainable Energy Rev.*, 16(5):2696–2723, Jun 2012.

[6] OLED Display Market Tracker - Q2 2018 - IHS Technology, Nov 2018. [Online; accessed 23. Nov. 2018].

[7] Sebastian Reineke, Frank Lindner, Gregor Schwartz, Nico Seidler, Karsten Walzer, Björn Lüssem, and Karl Leo. White organic light-emitting diodes with fluorescent tube efficiency. *Nature*, 459(7244):234, May 2009.

[8] Kazuki Kato, Toshihiko Iwasaki, and Takatoshi Tsujimura. Over 130 lm/w all-phosphorescent white oleds for next-generation lighting. *Journal of Photopolymer Science and Technology*, 28:335–340, 10 2015.

[9] J. S. Brown and S. E. Shaheen. Introducing correlations into carrier transport simulations of disordered materials through seeded nucleation: impact on density of states, carrier mobility, and carrier statistics. *J. Phys.: Condens. Matter*, 30(13):135702, Mar 2018.

[10] I. Yavuz. Dichotomy between the band and hopping transport in organic crystals: insights from experiments. *Physical Chemistry Chemical Physics*, 19(38):25819–25828, 2017.

[11] Harald Oberhofer, Karsten Reuter, and Jochen Blumberger. Charge Transport in Molecular Materials: An Assessment of Computational Methods. *Chem. Rev.*, 117(15):10319–10357, August 2017.

[12] Neil W Ashcroft. *Solid state physics*. Saunders College Publishing, Fort Worth, college ed. edition, 1976.

[13] Charles Kittel. *Introduction to solid state physics*. Wiley, New York, 7th ed edition, 1996.

[14] Matthew Habgood, Ricardo Grau-Crespo, and Sarah L. Price. Substitutional and orientational disorder in organic crystals: a symmetry-adapted ensemble model. *PCCP*, 13(20):9590–9600, May 2011.

[15] Thorsten Vehoff, Björn Baumeier, Alessandro Troisi, and Denis Andrienko. Charge Transport in Organic Crystals: Role of Disorder and Topological Connectivity. *J. Am. Chem. Soc.*, 132(33):11702–11708, Aug 2010.

[16] Fruzsina Gajdos, Harald Oberhofer, Michel Dupuis, and Jochen Blumberger. On the Inapplicability of Electron-Hopping Models for the Organic Semiconductor Phenyl-C61-butyric Acid Methyl Ester (PCBM). *J. Phys. Chem. Lett.*, 4(6):1012–1017, Mar 2013.

[17] R. A. Marcus and Norman Sutin. Electron transfers in chemistry and biology. *Biochimica et Biophysica Acta (BBA) - Reviews on Bioenergetics*, 811(3):265–322, Aug 1985.

[18] J. Spencer, F. Gajdos, and J. Blumberger. FOB-SH: Fragment orbital-based surface hopping for charge carrier transport in organic and biological molecules and materials. *The Journal of Chemical Physics*, 145(6):064102, August 2016.

[19] Jacob Spencer, Laura Scalfi, Antoine Carof, and Jochen Blumberger. Confronting surface hopping molecular dynamics with Marcus theory for a molecular donoracceptor system. *Faraday Discussions*, 195:215–236, 2016.

[20] Fruzsina Gajdos, Siim Valner, Felix Hoffmann, Jacob Spencer, Marian Breuer, Adam Kubas, Michel Dupuis, and Jochen Blumberger. Ultrafast Estimation of Electronic Couplings for Electron Transfer between pi-Conjugated Organic Molecules. *Journal of Chemical Theory and Computation*, 10(10):4653–4660, October 2014.

[21] M. E. Gershenson, V. Podzorov, and A. F. Morpurgo. Colloquium: Electronic transport in single-crystal organic transistors. *Rev. Mod. Phys.*, 78(3):973–989, Sep 2006.

[22] John C. Tully. Nonadiabatic Dynamics. pages 34–71.

[23] Simone Pisana, Michele Lazzeri, Cinzia Casiraghi, Kostya S. Novoselov, A. K. Geim, Andrea C. Ferrari, and Francesco Mauri. Breakdown of the adiabatic Born–Oppenheimer approximation in graphene. *Nat. Mater.*, 6(3):198, Feb 2007.

[24] M. Born and R. Oppenheimer. Zur Quantentheorie der Molekeln. *Ann. Phys.*, 389(20):457–484, Jan 1927.

[25] John C. Tully. Nonadiabatic molecular dynamics. *International Journal of Quantum Chemistry*, 40(S25):299–309, 1991.

[26] Todd J. Martínez∗. Insights for Light-Driven Molecular Devices from Ab Initio Multiple Spawning Excited-State Dynamics of Organic and Biological Chromophores. *American Chemical Society*, Oct 2005.

[27] Guillermo Albareda, Heiko Appel, Ignacio Franco, Ali Abedi, and Angel Rubio. Correlated Electron-Nuclear Dynamics with Conditional Wave Functions. *Phys. Rev. Lett.*, 113(8):083003, Aug 2014.

[28] John C. Tully. Molecular dynamics with electronic transitions. *J. Chem. Phys.*, 93(2):1061–1071, Jul 1990.

[29] R. L et al Whetten. Molecular dynamics beyond the adiabatic approximation: New experiments and theory. *Ann. Rev. Phys. Chem.*, 36:277–320.

[30] D. F. Coker and L. Xiao. Methods for molecular dynamics with nonadiabatic transitions. *J. Chem. Phys.*, 102(1):496–510, Jan 1995.

[31] John C. Tully. Perspective: Nonadiabatic dynamics theory. *The Journal of Chemical Physics*, 137(22):22A301, December 2012.

[32] Priya V. Parandekar and John C. Tully. Detailed Balance in Ehrenfest Mixed Quantum-Classical Dynamics. *Journal of Chemical Theory and Computation*, 2(2):229–235, March 2006.

[33] Federica Agostini, Seung Kyu Min, Ali Abedi, and E. K. U. Gross. Quantum-Classical Nonadiabatic Dynamics: Coupled- vs Independent-Trajectory Methods. *Journal of Chemical Theory and Computation*, 12(5):2127–2143, May 2016.

[34] Ali Abedi, Neepa T. Maitra, and E. K. U. Gross. Exact Factorization of the Time-Dependent Electron-Nuclear Wave Function. *Physical Review Letters*, 105(12), September 2010.

[35] Ali Abedi, Federica Agostini, Yasumitsu Suzuki, and E. K. U. Gross. Dynamical Steps that Bridge Piecewise Adiabatic Shapes in the Exact Time-Dependent Potential Energy Surface. *Physical Review Letters*, 110(26), June 2013.

[36] Oleg V. Prezhdo and Peter J. Rossky. Evaluation of quantum transition rates from quantum-classical molecular dynamics simulations. *J. Chem. Phys.*, 107(15):5863–5878, Oct 1997.

[37] Daniele Braga and Gilles Horowitz. High-Performance Organic Field-Effect Transistors. *Adv. Mater.*, 21(14-15):1473–1486, Feb 2009.

[38] Behzad Barış, Hatice Gürel Özdemir, Nihat Tuğluoğlu, Serdar Karadeniz, Ömer Faruk Yüksel, and Zeynep Kişnişci. Optical dispersion and dielectric properties of rubrene organic semiconductor thin film. *J. Mater. Sci. - Mater. Electron.*, 25(8):3586–3593, Aug 2014.

[39] Shree Prakash Tiwari, William J. Potscavage, Tissa Sajoto, Stephen Barlow, Seth R. Marder, and Bernard Kippelen. Pentacene organic field-effect transistors with doped electrode-semiconductor contacts. *Org. Electron.*, 11(5):860–863, May 2010.

[40] Tae-Young Kim, Jingon Jang, Kyungjune Cho, Younggul Song, Woanseo Park, Jinsu Park, Jae-Keun Kim, Woong-Ki Hong, and Takhee Lee. Interface effect in pentacene field-effect transistors from high energy proton beam irradiation. *Org. Electron.*, 27:240–246, Dec 2015.

[41] Samuele Giannini, Antoine Carof, and Jochen Blumberger. Crossover from Hopping to Band-Like Charge Transport in an Organic Semiconductor Model: Atomistic Nonadiabatic Molecular Dynamics Simulation. *The Journal of Physical Chemistry Letters*, 9(11):3116–3123, June 2018.

[42] Antoine Carof, Samuele Giannini, and Jochen Blumberger. Detailed balance, internal consistency, and energy conservation in fragment orbital-based surface hopping. *The Journal of Chemical Physics*, 147(21):214113, December 2017.

[43] Federica Agostini, Ali Abedi, Yasumitsu Suzuki, Seung Kyu Min, Neepa T. Maitra, and E. K. U. Gross. The exact forces on classical nuclei in non-adiabatic charge transfer. *The Journal of Chemical Physics*, 142(8):084303, February 2015.

[44] Federica Agostini, Seung Kyu Min, and E. K. U. Gross. Semiclassical analysis of the electron-nuclear coupling in electronic non-adiabatic processes. *Annalen der Physik*, 527(9-10):546–555, October 2015.

[45] Federica Agostini, Ali Abedi, Yasumitsu Suzuki, and E.K.U. Gross. Mixed quantum-classical dynamics on the exact time-dependent potential energy surface: a fresh look at non-adiabatic processes. *Molecular Physics*, 111(22-23):3625–3640, December 2013.

[46] Seung Kyu Min, Ali Abedi, Kwang S. Kim, and E. K. U. Gross. Is the Molecular Berry Phase an Artifact of the Born-Oppenheimer Approximation? *Phys. Rev. Lett.*, 113(26):263004, Dec 2014.

[47] Farnaz A. Shakib and Pengfei Huo. Ring Polymer Surface Hopping: Incorporating Nuclear Quantum Effects into Nonadiabatic Molecular Dynamics Simulations. *J. Phys. Chem. Lett.*, 8(13):3073–3080, Jul 2017.

[48] Basile F. E. Curchod, Ivano Tavernelli, and Ursula Rothlisberger. Trajectory-based solution of the nonadiabatic quantum dynamics equations: an on-the-fly approach for molecular dynamics simulations, Feb 2011.

[49] Ivano Tavernelli. Ab initio–driven trajectory-based nuclear quantum dynamics in phase space. *Phys. Rev. A*, 87(4):042501, Apr 2013.

[50] Arne Scherrer, Federica Agostini, Daniel Sebastiani, E. K. U. Gross, and Rodolphe Vuilleumier. Nuclear velocity perturbation theory for vibrational circular dichroism: An approach based on the exact factorization of the electron-nuclear wave function. *J. Chem. Phys.*, 143(7):074106, Aug 2015.

[51] Graeme H. Gossel, Federica Agostini, and Neepa T. Maitra. Coupled-Trajectory Mixed Quantum-Classical Algorithm: A Deconstruction. *Journal of Chemical Theory and Computation*, August 2018.

[52] J. VandeVondele, J; Hutter. Gaussian basis sets for accurate calculations on molecular systems in gas and condensed phases. *The Journal of Chemical Physics*, 127(11).

[53] Seung Kyu Min, Federica Agostini, Ivano Tavernelli, and E. K. U. Gross. Ab Initio Nonadiabatic Dynamics with Coupled Trajectories: A Rigorous Approach to Quantum (De)Coherence. *The Journal of Physical Chemistry Letters*, 8(13):3048–3055, July 2017.

[54] John C. Tully. Nonadiabatic Dynamics. pages 34–71, 1998.